

# We are IntechOpen, the world's leading publisher of Open Access books Built by scientists, for scientists

6,900

Open access books available

186,000

International authors and editors

200M

Downloads

Our authors are among the

154

Countries delivered to

TOP 1%

most cited scientists

12.2%

Contributors from top 500 universities



WEB OF SCIENCE™

Selection of our books indexed in the Book Citation Index  
in Web of Science™ Core Collection (BKCI)

Interested in publishing with us?  
Contact [book.department@intechopen.com](mailto:book.department@intechopen.com)

Numbers displayed above are based on latest data collected.  
For more information visit [www.intechopen.com](http://www.intechopen.com)



---

# Health Condition Monitoring of Induction Motors

---

Wilson Wang and Derek Dezhi Li

Additional information is available at the end of the chapter

<http://dx.doi.org/10.5772/61110>

---

## Abstract

Induction motors (IMs) are commonly used in various industrial applications. A spectrum synch (SS) technique is proposed in this chapter for early IM defect detection using electric current signals; fault detection in this work will focus on defects in rolling element bearings and rotor bars, which together account for more than half of IM imperfections. In bearing fault detection, the proposed SS technique will highlight the peakedness of the fault frequency components distributed over several fault related local bands. These bands are synchronized to form a fault information spectrum to accentuate fault features. A central kurtosis indicator is proposed to extract representative features from the fault information spectrum and formulate a fault index for incipient IM fault diagnosis. The effectiveness of the developed SS technique is tested on IMs with broken rotor bars and with damaged bearings.

**Keywords:** Induction motors, Bearing fault detection, Broken rotor bars, Current signal, Spectrum synch analysis

---

## 1. Introduction

Induction motors (IMs) are the workhorse of many industries such as manufacturing, mining, and transportation; and more importantly, they consume up to 50% of the generated electrical energy in the world [1]. Due to these facts, a series of R&D activities have been directed, for decades, to improve the performance and efficiency of IMs. For example, in industrial applications, an effective and reliable condition monitoring system is very valuable in the detection of an IM fault at its earliest stage in order to prevent performance reduction and malfunction of the driven machinery. It could also be utilized to schedule predictive maintenance.

nance operations without periodically shutting down machines for manual inspections. Maintenance costs can be further reduced (especially for large expensive motors) by quickly identifying the faulty component(s) without inspecting all components in the IM.

As illustrated in Figure 1, a typical IM consists of a stator, a rotor, a shaft, rolling element bearings, and the related supplementary components. IM components could be damaged during operations due to reasons such as impacts, fatigue, insufficient lubrication, aging, and so on. Investigations have revealed that bearing faults account for approximately 75% of small and medium-sized motor defects and 41% of large motor imperfections in domestic and industrial applications [2]. Other IM defects include broken rotor bars (up to 10%), stator winding faults, shaft imbalance, and phase imperfection.

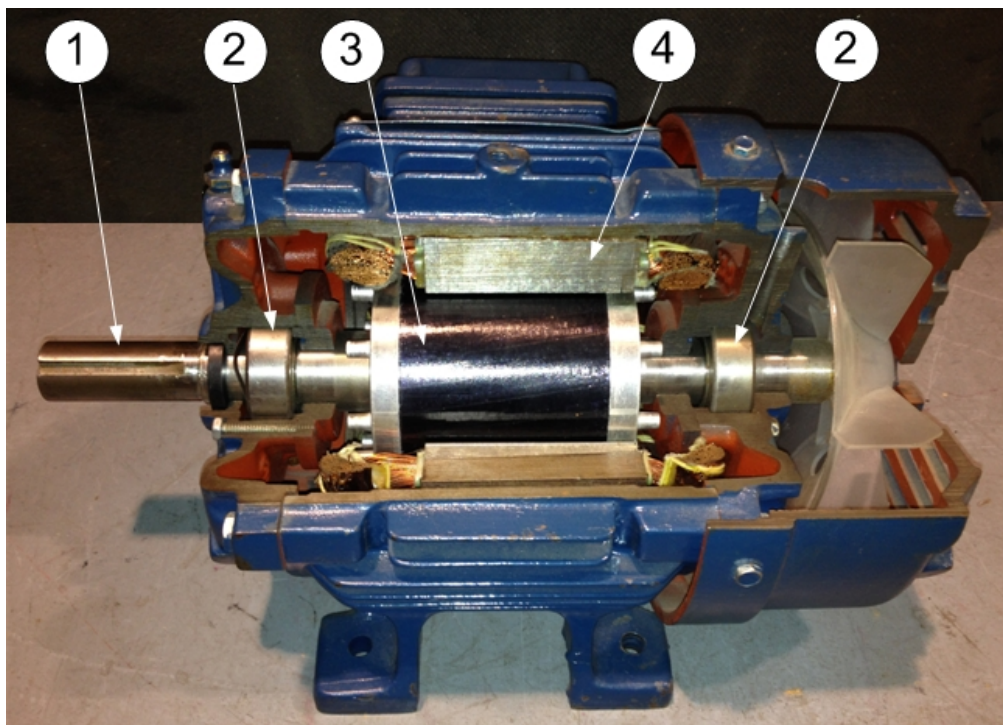


**Figure 1.** Structure of induction motors: 1-shaft, 2-bearings, 3-rotor, 4-stator.

The traditional IM fault diagnostic method, which is still widely practiced by maintenance crews in industry, relies on human diagnosticians for periodic inspections based on warning signs such as smell, temperature increase, excessive vibration, and increased acoustic noise level. However, these physical symptoms are prone to being contaminated with noise from other sources. The alternative is the use of signal processing techniques for fault detection. Signal processing is a process to extract representative features from the collected signals. Traditional machinery fault detection is based on thermal signals [3], acoustic signals, and vibration signals [4,5]. The local or bulk temperature can be used to diagnose IM defects, however the heat accumulation and progression are slow, which may not be suitable for incipient fault detection. The acoustic noise can indicate IM faults, especially for severe and distributed defects; however the acoustic signal is prone to contamination by background noise

such as noise from other machines in the vicinity. Vibration signals can be collected by the use of the related vibration sensors mounted in the vicinity of the IM support bearings. Although vibration signals have relatively high signal-to-noise ratio, the vibration sensors are expensive and require a high degree of installation accuracy. The alternative is to use the stator current signal for analysis, which is non-invasive to the IM structure. In addition, electric current sensors are inexpensive and easy to install [6]. Thus, the proposed research in this work will focus on IM fault diagnosis using stator current signals.

Several motor current signature analysis techniques have been proposed in the literature for fault detection in IMs, mainly for rotors and bearings, which are briefly summarized next.

### **1.1. Fault detection of IM rotors**

Broken rotor bars are common rotor defects that will render asymmetries of an IM rotor. The rotor bar failures can be caused by several factors, such as overheating due to frequent starts under loading, unbalanced thermal load due to air gap eccentricity, manufacturing defects, and corrosion of rotor material caused by chemicals or moisture [7].

Because of the aforementioned reasons, the rotor bar(s) may be fully or partially damaged, which will cause the rotor cage asymmetry and result in asymmetrical distribution of the rotor currents. When a crack forms in a rotor bar, the cracked bar will overheat and tend to break. Then the adjacent bars have to carry higher currents and consequently they become prone to damage, leading to multiple bar fractures. Moreover, the broken parts from the faulty bars may hit the end winding of the motor and cause serious mechanical damage to the IM [8].

The Fast Fourier Transform (FFT) spectral analysis is a commonly used method for rotor bar breakage detection, by examining the characteristic frequency components in the spectrum. For example, Elkasabgy et al. [9] used spectral analysis of IM current signals to detect rotor bar breakage. It has been reported that the IM current signal becomes non-stationary if rotor bars are damaged. However, the FFT is useful for stationary signal analysis only, which lacks the capability of capturing the transitory characteristics such as drifts, abrupt changes, and frequency trends in non-stationary signals. To solve the problem, time-frequency methods, such as short time Fourier transform (STFT), can be used to process small segments of non-stationary signals for broken rotor bar defect detection. For example, Arabaci and Bilgin [10] applied the STFT to detect IM rotor bar faults. However, the STFT cannot provide the information corresponding to different time resolutions and frequency resolutions due to its fixed length windowing functions [11]. To solve this problem, the wavelet transform (WT) can be employed to explore the information associated with different frequency resolutions. For example, Daviu et al. [12] used discrete WT to detect IM broken rotor bars fault. The wavelet packet decomposition (WPD) was used to explore the whole frequency band with high resolution. For example, Sadeghian et al. [13] used WPD to extract features and applied neural networks to diagnose IM rotor bar breakage. Pineda-Sanchez et al. [14] employed polynomial-phase transform to diagnose broken rotor bar fault in time-varying condition. Riera-Guasp et al. [15] extracted broken rotor bar fault features from transient state of IM using Gabor analysis. Although the WPD can explore details of the signal for some advanced signal analysis, it is usually difficult to recognize the real representative features from the map with redundant

and misleading information. Akin et al. [16] performed real-time fault detection using the reference frame theory. Soualhi et al. [17] diagnosed broken rotor bar fault through the classification of selected fault features using the improved artificial ant clustering method. Gunal et al. [18] conducted IM broken rotor bar fault diagnosis by using fault indices in the time domain. Nevertheless, the aforementioned techniques only focus on limited fault information, thus their performance may be degraded.

## 1.2. Fault detection of IM bearings

Rolling element bearings are commonly used not only in electric motors, but also in various types of rotating machinery facilities. As illustrated in Figure 2, a rolling element bearing is a system consisting of an outer ring (usually the fixed ring), an inner ring (usually the rotating ring), a number of rolling elements, and a cage.

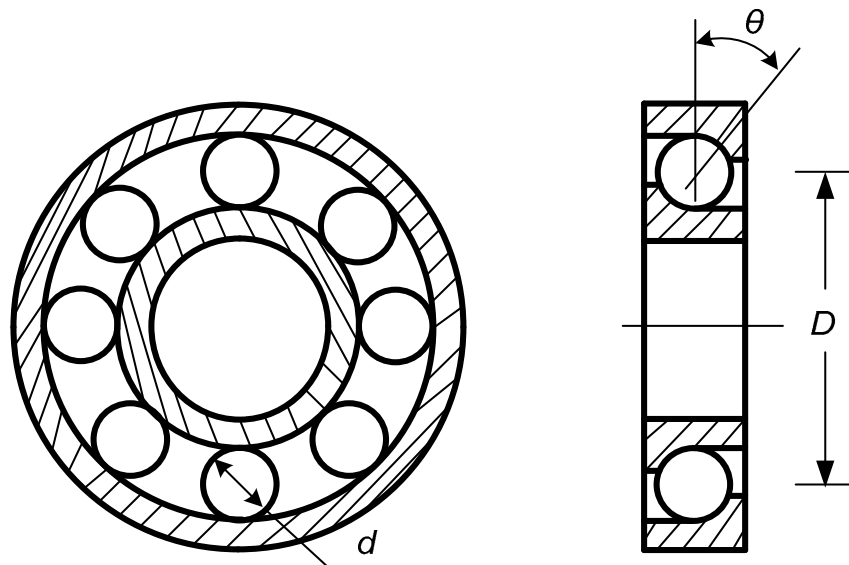


**Figure 2.** Structure of a rolling element bearing.

Since bearing materials are subjected to dynamic loading, fatigue pitting is the most common defect in bearing components. The bearing defects can occur on the outer race, inner race, and rolling elements. Under normal operating conditions, after the load cycles exceed some threshold, fatigue pitting may occur on the fixed ring race first, and then on the rotating race and rolling elements. Pitting defects not only deteriorate transmission accuracy, but also generate excessive vibration and noise. Other bearing defects, such as scoring and severe wear [7], can be generated by several external causes such as impacts, overloading and overheating, inadequate lubrication, contamination and corrosion from abrasive particles or acid, and improper installation of a bearing, which will introduce excessive misalignment errors.

When a bearing component is damaged, the corresponding characteristic frequencies will be associated with the bearing geometry, rotation speed, and defect location. Suppose the outer

race of a bearing is fixed and the inner race rotates with the shaft, which is common case in most applications. The outer race defect characteristic frequency  $f_{od}$  inner race defect characteristic frequency  $f_{id}$  and rolling element defect characteristic frequency  $f_{rd}$  are determined by

$$f_{od} = \frac{N}{2} \left[ f_i \left( 1 - \frac{d \cos(\theta)}{D} \right) \right] \quad (1)$$

$$f_{id} = \frac{N}{2} \left[ f_i \left( 1 + \frac{d \cos(\theta)}{D} \right) \right] \quad (2)$$

$$f_{rd} = \frac{D}{2d} f_i \left[ 1 - \left( \frac{d \cos \theta}{D} \right)^2 \right] \quad (3)$$

where  $f_i$  is the inner race rotating speed or shaft speed in Hz;  $d$  is the diameter of the rolling element;  $D$  is the pitch diameter;  $\theta$  is the contact angle.

When bearing defects occur, these bearing characteristic vibration frequencies  $f_v$  (i.e.,  $f_{od}$ ,  $f_{id}$  and  $f_{rd}$ ) will be modulated with the power supply frequency  $f_p$  in the spectrum of stator current signals, because of the air gap eccentricity and load torque variations. Thus, the characteristic stator current frequencies  $f_c$  in terms of characteristic vibration frequencies  $f_v$  will be calculated by [19]:

$$f_c = \left| f_p \pm m f_v \right|, m = 1, 2, 3, \dots \quad (4)$$

For IM bearing fault detection, the characteristic stator current frequency components can be used as frequency domain indicators in spectrum analysis [20]. Several techniques have been proposed in the literature for IM bearing fault detection using stator current signals. For example, Devaney and Eren [21] applied IM stator current spectrum analysis for bearing defect detection. FFT can be used to conduct spectrum analysis, so as to detect IM bearing faults under deterministic motor conditions. Similar to the previous discussion regarding broken rotor bar analysis, the WT can be used to catch the transitory characteristics of the signal for IM bearing fault detection. For example, Konar and Vhattopadhyay [22] employed discrete WT to detect IM bearing faults. The WPD can also be employed to explore transient fault information for IM bearing fault detection [23]. Nevertheless, the WPD generates massive non-fault-related information that may mask the fault features in the map, and increase the difficulties in fault detection. Frosini and Bassi [24] used features from stator current signals and IM efficiency for bearing fault detection. Zhou et al. [25] utilized the Wiener filter for noise reduction, so as to detect IM bearing defect. Romero-Troncoso et al. [26] conducted online IM fault detection using

information entropy and fuzzy inference. Pineda-Sanchez et al. [27] employed Teager-Kaiser energy operator to enhance fault features to detect IM bearing defect. Nevertheless, these available techniques conduct IM bearing fault detection based on limited fault information rather than comprehensively explore fault features from the time domain, the frequency domain, and the time-frequency domain. Therefore their performance may be degraded.

Typically, the onset of IM faults begins with small imperfections, and propagates to a severe stage as the operation progresses. The severe IM faults will cause machinery malfunction, and even catastrophic failures. Therefore, the detection of IM faults at their earliest stage is of great importance in IM condition monitoring. The IM fault features from stator current signals would be associated with fault size, motor type, supply frequency, load condition, and so on. To date, fault feature extraction from IM current signals, especially associated with bearing defects, still remains a challenging task due to the complex transmission path and environmental noise.

To tackle the aforementioned difficulties, a spectrum synch (SS) technique is proposed in this work to gather fault-related information and generate representative features of IM faults, such as broken rotor bar fault and outer race defect in a bearing. The SS will examine characteristic frequency components as well as their features over their neighborhood local bands, in order to comprehensively highlight fault features, and mitigate the effects of high amplitude outliers. The specific approaches in the proposed SS technique include the following: (1) a synch technique is proposed to form fault information spectrum (FIS) by synchronizing several fault-related local bands, so as to accentuate the fault features and improve the SNR; (2) a central kurtosis technique is suggested to extract fault information from the resulting FIS and generate a fault indicator for incipient IM fault detection. The effectiveness of the proposed SS technique is verified by IM broken rotor bar fault detection and IM bearing fault detection.

The remainder of this chapter is organized as follows: the developed SS technique is described in Section 2. The effectiveness of the proposed diagnostic tool is examined in Section 3 by using two common types of IM fault conditions; finally, some concluding remarks of this study are summarized in Section 4.

## **2. The spectrum synch technique for IM health condition monitoring**

### **2.1. Theory of spectrum synch analysis**

The proposed SS technique is composed of two procedures: local band synch and central kurtosis analysis. The local band synch is used to form the fault information spectrum (FIS) and accentuate fault features. The central kurtosis is suggested to generate fault indices for IM health condition monitoring.

#### *2.1.1. Local band synch*

The IM fault characteristic frequency components are distributed over the spectrum, which, however, are usually difficult to recognize due to their low amplitude. To highlight fault

features in the spectrum, the FIS is used to enhance the local peakedness of the fault frequency components. Firstly, to mitigate the noise effect in the IM current signal, the spectrum averaging of  $J$  data sets  $\varphi_j, j = 1, 2, \dots, J$ , is applied to improve the signal-to-noise ratio (SNR), computed by

$$\Phi = \frac{1}{J} \sum_{j=1}^J \log(P(\varphi_j)) \quad (5)$$

where  $\Phi$  is the averaged spectrum over  $J$  spectra;  $P(\varphi_j)$  represents the nonparametric power spectral density (PSD) estimate of the data set [28], given by

$$P(\varphi_j) = \frac{2}{f_s N} \sum_{i=1}^{N/2+1} |F_j(i)|^2 \quad (6)$$

where  $F_j$  is the spectrum of  $\varphi_j$  using the Fourier transform (FT);  $N$  is the length of  $\varphi_j$ ; and  $f_s$  is the sampling frequency.

The fault features are related to fault characteristic frequencies, most of which are masked over the local bands by some other higher level frequency components considered as noise. To tackle this problem, the local bands containing the fault characteristic frequencies are synchronized to reduce the noise effect and protrude the fault frequency components. In each selected local band, the fault frequency component  $f_c$  is located in the center of the window, and the width of the local band is selected to properly reveal the peakedness of  $f_c$ .

To synchronize the corresponding bands at different locations (frequencies) of the spectrum, the spectrum is transformed from the frequency domain  $\Phi(f)$  to discrete point representation  $\Phi(d)$ . Each frequency  $f$  can be represented by its nearest discrete point  $d$ . Then, fault characteristic frequency  $f_c(k)$  is transformed into a discrete point,  $d_c(k)$ , whose corresponding frequency is the one closest to  $f_c$ , where  $k = 1, 2, \dots, K$ , and  $K$  is the total number of fault characteristic frequencies considered. Thus,  $K$  local bands will be used for this synch operation. The widths of local bands are identical in this work to facilitate the synch operation. Given the bandwidth in frequency  $f_w$  the length of the local band in discrete point representation,  $d_w$  will be

$$d_w = 2R \left\langle \frac{1}{2} f_w \frac{D_s}{f_s} \right\rangle \quad (7)$$

where  $f_s$  is the sampling frequency in Hz,  $D_s$  is the discrete point representing  $f_s$ , and  $R \langle \cdot \rangle$  represents round-off operation. The  $k^{\text{th}}$  local band  $\psi_k$  in the discrete point representation can be determined by

$$\psi_k = \left\{ \Phi(i) \right\}_{i=d_c(k)-\frac{1}{2}d_w, \dots, d_c(k)+\frac{1}{2}d_w} - \frac{1}{d_w+1} \sum_{i=d_c(k)-\frac{1}{2}d_w}^{d_c(k)+\frac{1}{2}d_w} \Phi(i) \quad (8)$$

The  $i^{\text{th}}$  discrete point in the  $k^{\text{th}}$  local band  $\psi_k$  is denoted as  $\psi_{i,k}$ ,  $i = 1, 2, \dots, d_w+1$ ;  $k = 1, 2, \dots, K$ . The  $i^{\text{th}}$  discrete points over  $K$  local bands  $\{\psi_{i,k}\}$  are sorted in a descending order in terms of their values to generate  $\pi_{i,k}$ ,  $k = 1, 2, \dots, K$ ; the synchronized band FIS will be

$$g_i = \begin{cases} \frac{2}{(K-1)} \sum_{j=1}^{(K-1)/2} \pi_{i,j} & K \text{ is odd} \\ \frac{2}{K} \sum_{j=1}^{K/2} \pi_{i,j} & K \text{ is even} \end{cases}, i = \frac{1}{2}d_w + 1 \quad (9)$$

$$g_i = \xi \left\{ \pi_{i,j} \right\}_{j=1, 2, \dots, K}, i = 1, 2, \dots, \frac{1}{2}d_w, \frac{1}{2}d_w + 2, \dots, d_w + 1 \quad (10)$$

where  $\xi \{\cdot\}$  represents the computation of median value. The top 50% high amplitude center frequency components in local bands are averaged in Equation (9) to enhance the fault feature. The median value calculation in Equation (10) will suppress other frequency components in local bands and reduce the amplitude of outliers. The processing procedures of the proposed FIS formation are illustrated in Figure 3, where the frequency resolution  $\Delta f = 0.5$  Hz.

## 2.2. Central kurtosis analysis

The classic kurtosis is a measure of the peakedness of a signal, computed as  $\chi = \frac{\mu_4}{\sigma^4}$ , where  $\sigma$  and  $\mu_4$  are the standard deviation and the fourth moment of the signal distribution, respectively. The classic kurtosis measures all peaked frequency components of the FIS, which may not properly reveal the fault information. In this work, the fault detection aims to evaluate the peakedness of the center frequency component in the FIS. Therefore, a central kurtosis indicator is proposed to facilitate fault detection. Given the FIS  $g(i)$ ;  $i = 1, 2, \dots, d_w+1$ , the relative amplitude of the center frequency components can be determined by

$$v_s = g_s - \xi \{g\} \quad (11)$$

where  $g_s = \{g_i\}_{i=d_w/2+1}$  is the center discrete point in the FIS. The amplitude of fault frequency component over synchronized local bands (i.e., FIS), rather than the entire spectrum as in the classical methods, is used to examine fault information.

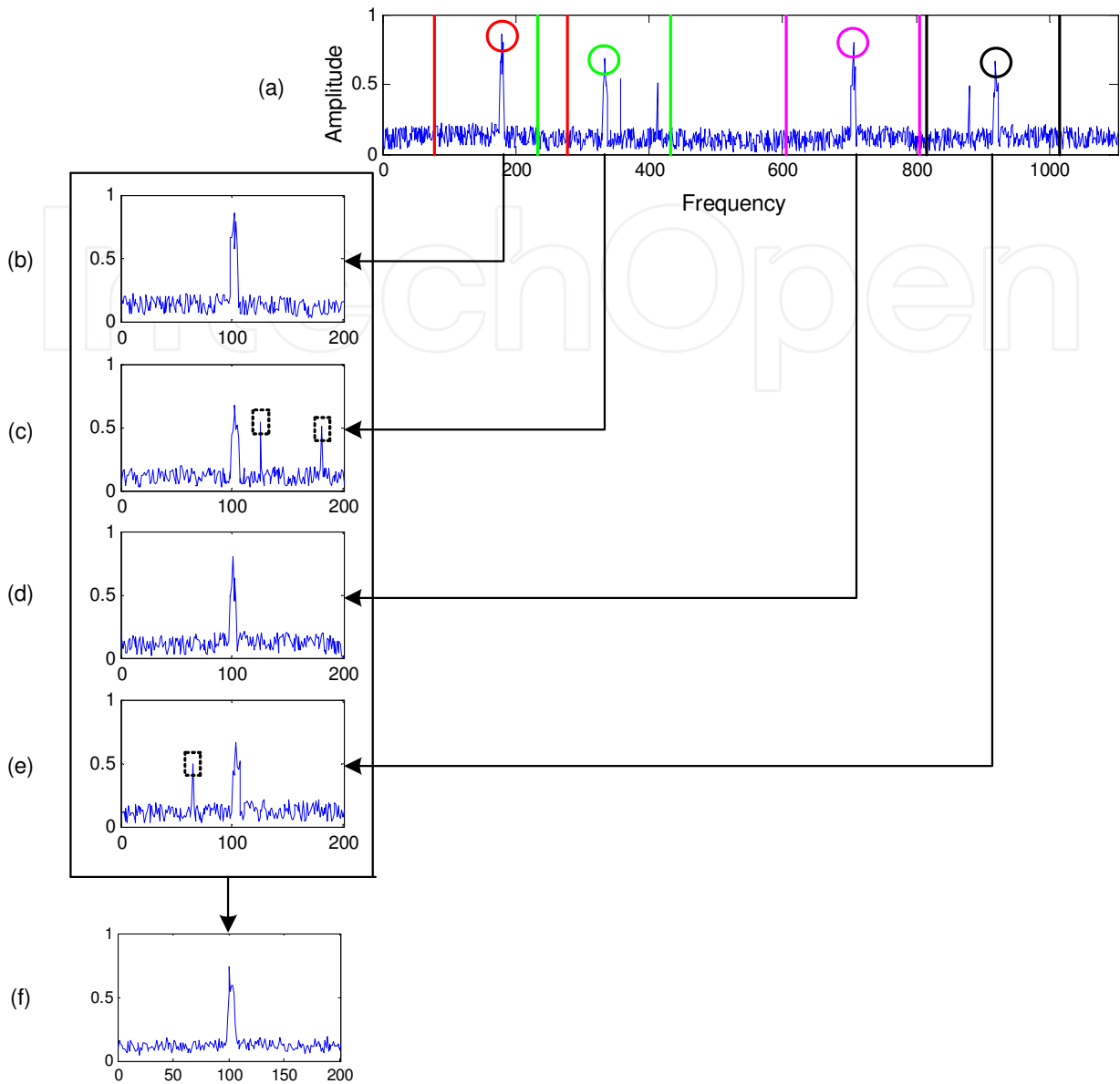


**Figure 3.** The formulation of FIS: (a) is the original spectrum; (b)-(e) are respective extracted local bands corresponding to the four circled fault frequency components (red, green, pink, and black); (f) is the formulated FIS. The dotted lines in graph (a) represent the boundaries of the local bands; the dashed rectangular boxes represent outliers in the local bands.

The variation of the FIS excluding center frequency component  $g_s$  can be evaluated by

$$\sigma_s = E\left\{\left(\tilde{g} - \xi\{\tilde{g}\}\right)^2\right\}^{\frac{1}{2}} \quad (12)$$

where  $E\{\cdot\}$  represents the expectation function, and  $\tilde{g} = \{g_i, i=1, 2, \dots, d_w/2, d_w/2+2, \dots, d_w+1\}$ .

Then the peakedness of the fault frequency component in the FIS can be measured by the central kurtosis, determined by

$$\chi_s = \begin{cases} v_s^4 / \sigma_s^4 & \text{if } v_s > 0 \\ 0 & \text{if } v_s \leq 0 \end{cases} \quad (13)$$

### 2.3. Implementation of Spectrum Synch Technique

To recapitulate, the proposed SS technique is implemented for IM defect detection in the following steps:

- a. Collect  $J$  electric current data sets  $\varphi_j$ ,  $j = 1, 2, \dots, J$ , with the same time delay.
- b. Determine the spectrum average  $\Phi$  over  $J$  spectra. Then extract characteristic local bands using Equation (8). Synchronize the local bands to form the FIS using Equations (9) and (10), in order to reduce the noise effect and highlight fault features.
- c. Compute the center frequency representative feature using Equation (11), and the variation of the FIS using Equation (12). The fault diagnosis can be performed by analyzing the central kurtosis computed from Equation (13).

## 3. Performance evaluation

To evaluate the effectiveness of the proposed SS technique for IM fault detection, a series of tests have been conducted for the two common types of IM defects, IM broken rotor bar fault and IM bearing defect, using stator current signals. In rolling element bearings, defect occurs on the race of the fixed ring first since fixed ring material over the load zone experiences more cycles of fatigue loading than other bearing components (i.e., the rotating ring and rolling elements). Correspondingly, this test focuses on incipient bearing defect, or fault on the outer race (fixed ring in this case). The tests are conducted for two power supply frequencies  $f_p$ :  $f_p = 35$  Hz and 50 Hz.

### 3.1. Experimental setup

Figure 4 shows the experimental setup employed in the current work. The speed of the tested IM is controlled by a VFD-B AC speed controller (from Delta Electronics) with output frequency 0.1~400 Hz. A magnetic particle clutch (PHC-50 from Placid Industries) is used as a dynamometer for external loading. Its torque range is from 1 to 30 lb ft (1.356-40.675 N m). The motor used for this research is made by Marathon Electric, and its specifications are summarized in Table 1. The gearbox (Boston Gear 800) is used to adjust the speed ratio of the dynamometer. The current sensors (102-1052-ND) are used to measure different phase currents. A rotary encoder (NSN-1024) is used to measure the shaft speed with the resolution

of 1024 pulses per revolution. Stator current signals are collected using a Quanser Q4 data acquisition board, which are then fed to a computer for further processing.

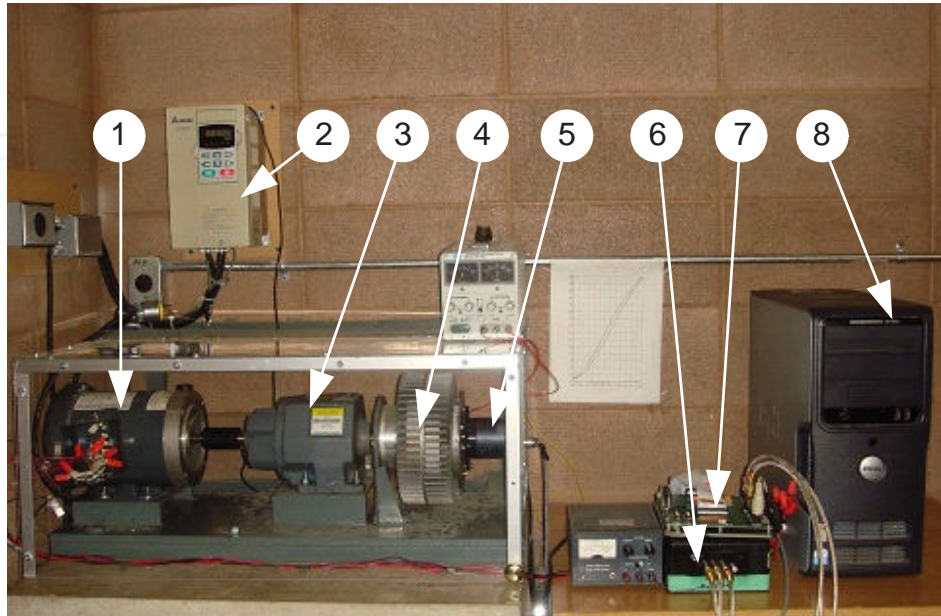


**Figure 4.** IM experimental setup: (1) tested IM, (2) speed controller, (3) gearbox, (4) load system, (5) encoder, (6) current sensors, (7) data acquisition system, and (8) computer.

Phase	3	Connection	Y
Poles	2	RPM	2850
HP	1/3	Rotor Bars	34
HZ	50	Stator Slots	24

**Table 1.** Motor specifications.

### 3.2. Broken rotor bar fault detection

The fault detection of IM broken rotor bar defect is generally based on spectral analysis by inspecting fault-related sideband components in the spectrum:

$$f_{bl} = (1 - 2ks) f_p \quad (14)$$

$$f_{br} = (1 + 2ks) f_p \quad (15)$$

where  $f_{bl}$  and  $f_{br}$  are the respective left sideband and right sideband of the IM broken rotor bar fault,  $k = 1, 2, \dots$ ;  $f_p$  is the power supply frequency of the IM;  $s = \frac{n_s - n_a}{n_s} \times 100\%$  is the slip of the IM.  $n_s$  (rpm) is the speed of rotating magnetic field, and  $n_a$  (rpm) is the shaft rotating speed. In the following tests, an IM containing three broken rotor bars is used to evaluate the proposed SS technique.

To examine the effectiveness of the proposed SS technique, the power spectral density (PSD) based fault detection and the envelope analysis based fault detection are used for comparison. The PSD explores the energy distribution of the data over the spectrum; the envelope analysis performs amplitude demodulation to reveal fault features. In the PSD-based fault detection, the fault index can be represented as,

$$\chi_p = \begin{cases} v_p^4 / \sigma_p^4 & \text{if } v_p > 0 \\ 0 & \text{if } v_p \leq 0 \end{cases} \quad (16)$$

The fault index of envelope analysis is given as

$$\chi_e = \begin{cases} v_e^4 / \sigma_e^4 & \text{if } v_e > 0 \\ 0 & \text{if } v_e \leq 0 \end{cases} \quad (17)$$

where  $v_p$  and  $v_e$  represent the averages of the top 50% high amplitude fault frequency components from PSD and envelope analysis respectively;  $\sigma_p$  and  $\sigma_e$  represent the standard deviations of the entire spectrum band of interests from PSD and envelope analysis respectively;  $\chi_p$  and  $\chi_e$  are the respective fault indices from PSD and envelope analysis. Therefore, these two techniques can be used to compare the local band synch method in the proposed SS technique, and the corresponding central kurtosis index.

### 3.2.1. 35 Hz supply frequency

The first test aims to detect the IM with three adjacent broken rotor bars, 35 Hz power supply frequency, and a half load (50% of rated power). To reduce the noise effect in the spectrum, twenty data sets are collected for spectrum averaging (i.e.,  $J = 20$ ). Other settings are  $f_s = 65,500$  Hz and  $f_w = 10$  Hz. Since 1,024 low-to-high voltage transitions represent one shaft revolution in the encoder signal, the high sampling frequency  $f_s$  is chosen to properly capture the encoder signal, so as to accurately estimate shaft speed (i.e., rotor speed). The frequency band [25 Hz, 45 Hz] is used to detect broken rotor fault, because the amplitudes of high order (i.e.,  $k$  in Equations (14) and (15)) characteristic frequencies are not prominent in the spectrum. Figure 5 illustrates the PSD of a healthy IM (Figure 5a), the PSD of an IM with broken rotor bars (Figure 5b), the envelope analysis of a healthy IM (Figure 5c), and the envelope analysis of an IM with broken rotor bars (Figure 5d), respectively. From Figures 5(b) and 5(d), it is seen that the broken rotor bar fault frequency components, although visible, do not prominently

protrude in the spectrum. Therefore, a better fault detection technique is needed to extract useful information from multiple characteristic frequency components in the spectrum to generate a more reliable fault index.

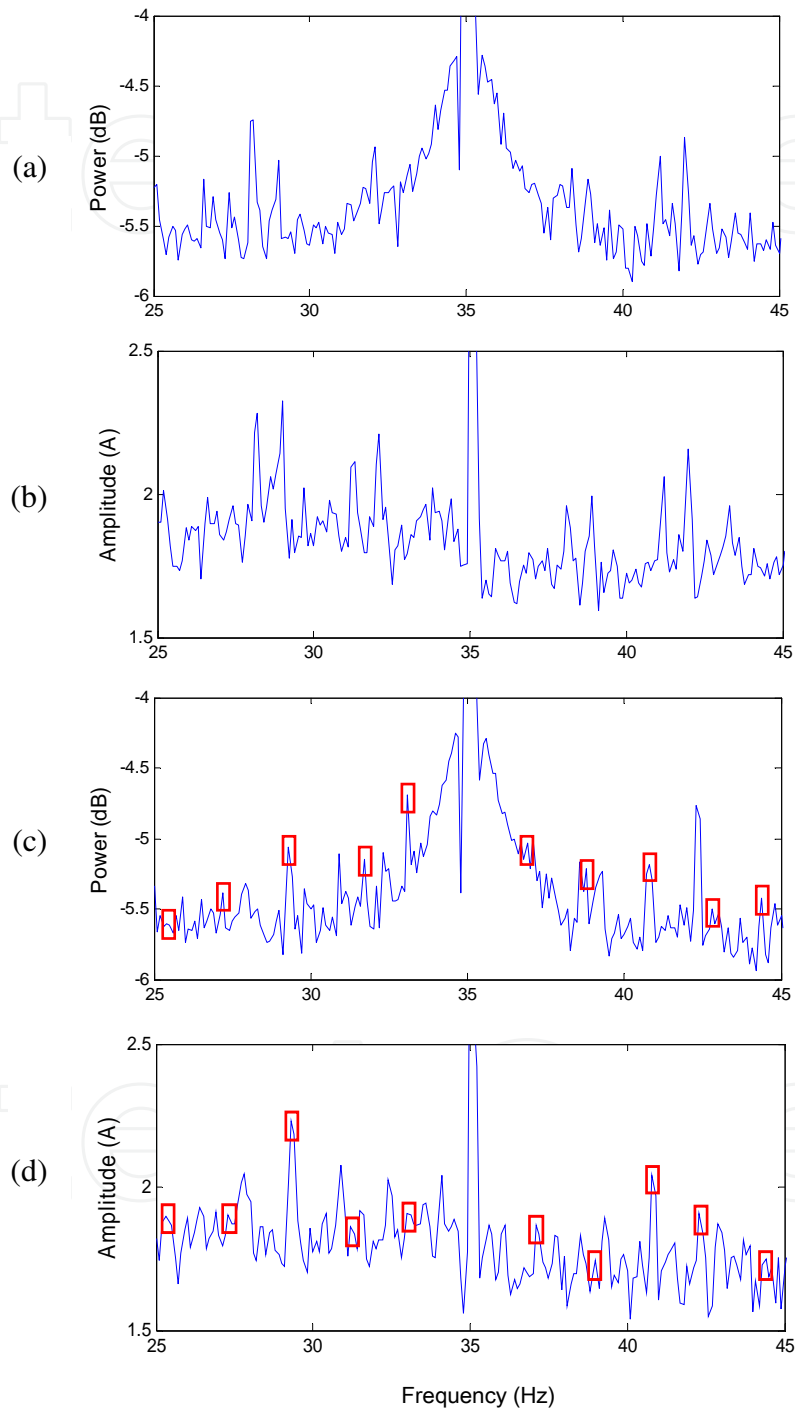


**Figure 5.** The spectrum average  $\Phi$  corresponding to: (a) a healthy IM using PSD; (b) an IM with broken rotor bar fault using PSD; (c) a healthy IM using envelope analysis; and (d) an IM with broken rotor bar fault using envelope analysis, at 35 Hz supply frequency and medium-load condition. The red solid rectangular boxes in (b) and (d) highlight fault frequency components.

The FIS, corresponding to a healthy IM (Figure 5a) and a broken rotor bar faulted IM (Figure 5b), are given in Figures 6(a) and 6(b), respectively. The unit of amplitude of the FIS is dB because the local bands are extracted from the PSD logarithmic spectrum. It is seen from Figure 6 that the center frequency component (i.e., synchronized broken rotor bar fault frequency components) in Figure 6(b) has higher relative amplitude than that in Figure 6(a), which is evaluated by the index  $\nu_s$  in the proposed SS technique. Figure 6(b) has similar spectrum variation as in Figure 6(a), which is examined by the value  $\sigma_s$  in the SS technique. Therefore, the fault information in the FIS can be characterized by the index  $\chi_s$  using the proposed SS technique.

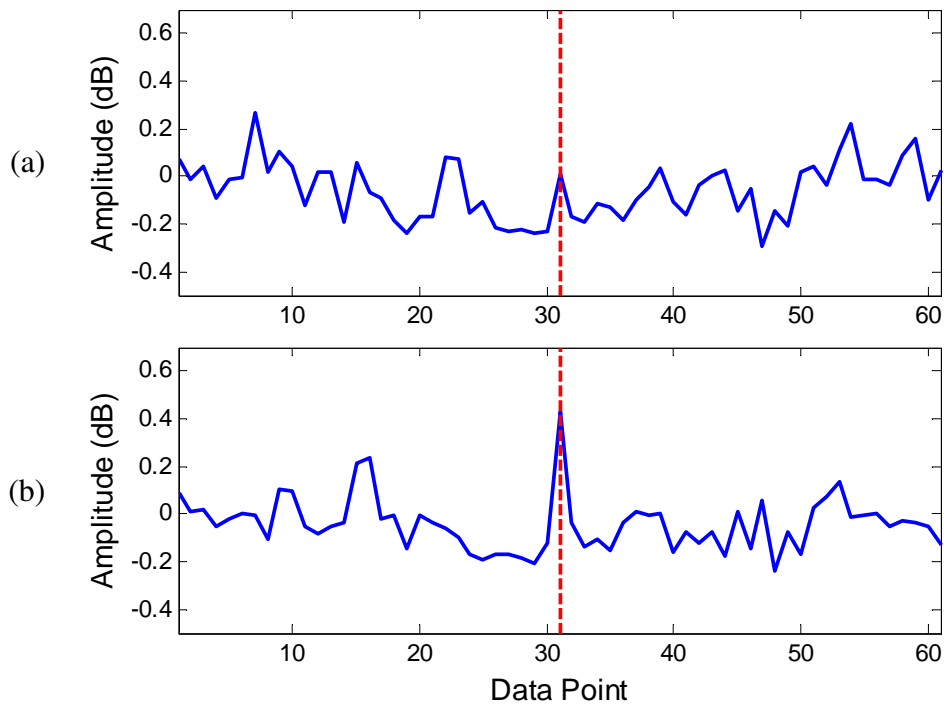


**Figure 6.** The FIS generated by the SS technique at 35 Hz and a half load condition: (a) from a healthy IM, (b) from an IM with broken rotor bar fault.

The values of IM speed  $f_r$  (Hz) and indices corresponding to PSD, envelope analysis and the proposed SS are summarized in Table 2. It is seen from Table 2 that it is difficult to differentiate the IM broken rotor bar faulted condition from the IM healthy condition using envelope analysis, because the values of  $\chi_e$  corresponding to these two IM conditions are similar. The PSD has a relatively large difference of  $\chi_p$  of different IM conditions in this case; however, the PSD suffers from interference of non-fault-related high amplitude frequency components and its  $\chi_p$  values are too small to be relied on. The IM with broken rotor bar defect has considerably larger value of  $\chi_s$  than that of the healthy IM using the proposed SS technique. Consequently, the proposed SS technique associated with its index  $\chi_s$  can be used as a fault index for IM broken rotor bar fault detection in the stator current spectrum.

Methods	PSD		Envelope analysis		SS	
	Healthy	Faulty	Healthy	Faulty	Healthy	Faulty
$f_r$	34.333	34.343	34.333	34.343	34.333	34.343
$V_p; V_e; V_s$	0.012	0.289	0.132	0.159	0.048	0.472
$\sigma_p; \sigma_e; \sigma_s$	0.751	0.764	0.176	0.161	0.122	0.098
$\chi_p; \chi_e; \chi_s$	6.519e-8	0.021	0.316	0.951	0.024	538

**Table 2.** Comparisons of central kurtosis indices for IM broken rotor bar fault detection.

### 3.2.2. 50 Hz supply frequency

The proposed SS technique is then used for IM broken rotor bar fault detection with 50 Hz supply frequency and a half load condition (50% of rated power). Other settings remain the same as in the previous tests. The spectrum of frequency band [35, 65] Hz is used for fault diagnosis. The selected band is shown in Figure 7 using PSD in Figure 7(a) and the envelope analysis in Figure 7(b), respectively. It is seen from Figure 7 that most of the fault frequency components are masked by noise, which cannot be used effectively for reliable fault diagnosis.

The FIS, corresponding to a healthy IM and an IM with broken rotor bar fault are given in Figures 8(a) and 8(b), respectively. The related IM condition indices are summarized in Table 3. It is seen that the relative amplitude of fault frequency component in Figure 8(b) is greater than that in Figure 8(a). From Table 3, the IM with broken rotor bar fault has a larger value of  $\chi_s$  than that of a healthy IM, which indicates a broken rotor bar fault. The IM health condition with broken rotor bars cannot be differentiated from healthy condition using envelope analysis, associated with its fault index  $\chi_e$ . Although the PSD index  $\chi_p$  has a relatively large difference corresponding to different IM conditions, the performance of PSD may be degraded by the interference of non-fault-related high amplitude frequency components and its  $\chi_p$  values are too small to be relied on. Hence, the proposed SS technique associated with its fault index  $\chi_s$  can accurately discern the health condition of IMs with broken rotor bar fault under different supply frequencies, when compared to the related two classical methods.

### 3.3. Incipient bearing defect detection

As mentioned earlier, bearing defects are the most common faults in IMs, which also represent the most challenging task in IM health condition monitoring, especially when using stator current signals [29]. A small dent of diameter approximately 1/16-inch was introduced on the outer race of the bearing to simulate fatigue pitting defect. Whenever a rolling element rolls over the damaged region, impulses are generated, which then excite the resonance frequencies of the IM structures. The vibration-related outer race bearing defect characteristic frequency  $f_v$  is given in Equation (1). The corresponding characteristic current frequency  $f_c$  can be calculated using Equation (4).

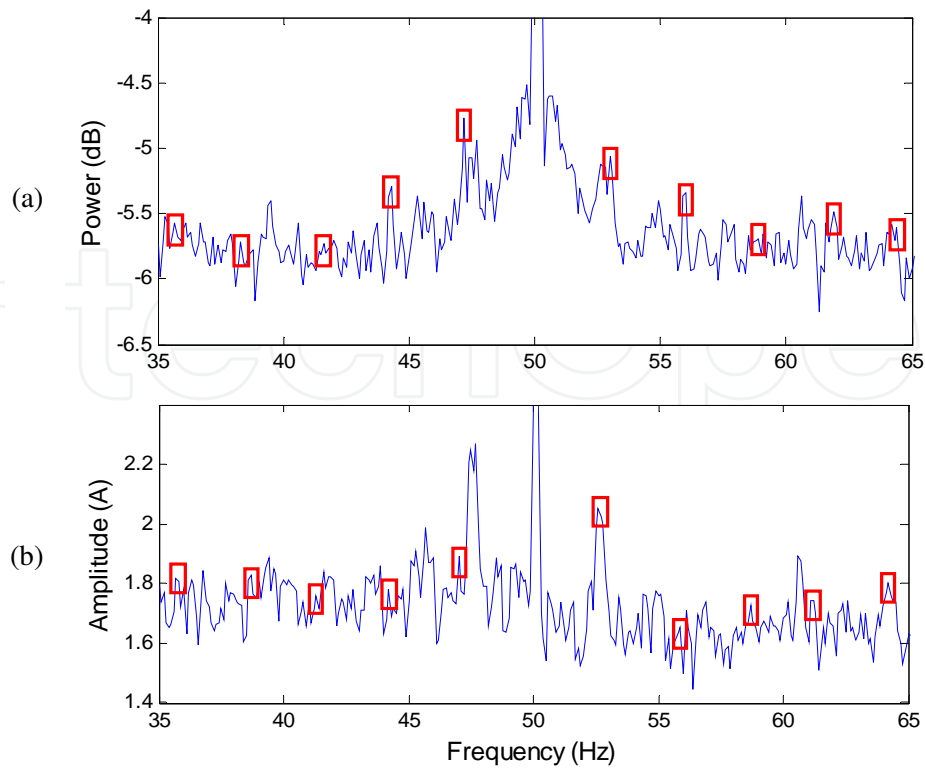


**Figure 7.** The spectrum  $\Phi$  for an IM with broken rotor bar fault, 50 Hz supply frequency and half-load condition, using: (a) PSD; and (b) envelope analysis. The red solid rectangular boxes highlight fault frequency components.

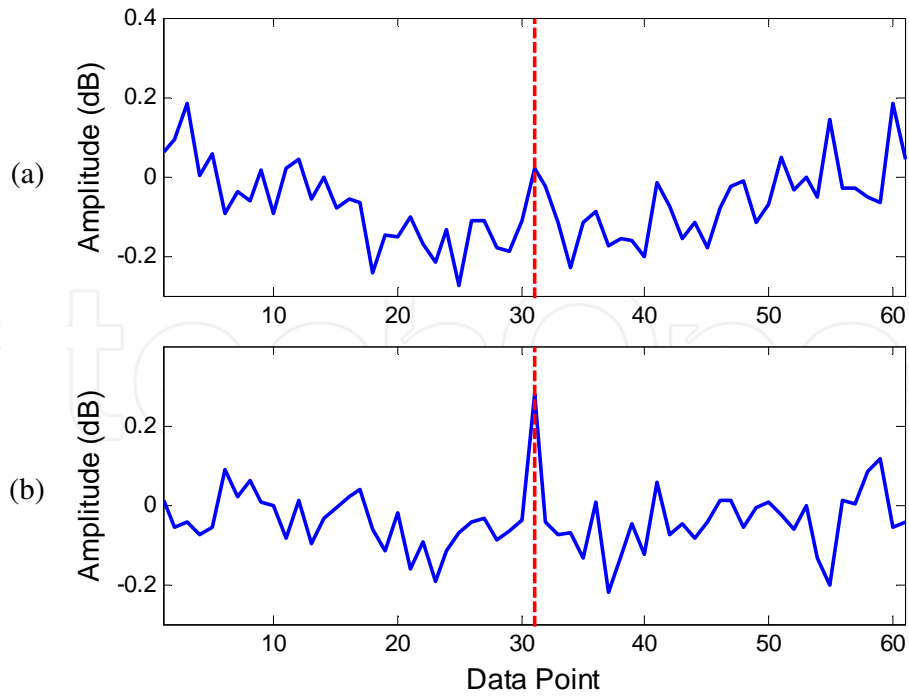


**Figure 8.** The FIS generated by the SS technique at 50 Hz supply frequency and a half-load level (a) from a healthy IM; (b) from an IM with broken rotor bars.

Methods	PSD		Envelope analysis		SS	
	Healthy	Faulty	Healthy	Faulty	Healthy	Faulty
$f_r$	49.180	49.089	49.180	49.089	49.180	49.089
$v_p; v_e; v_s$	0.103	0.195	0.083	0.119	0.092	0.325
$\sigma_p; \sigma_e; \sigma_s$	0.634	0.653	0.149	0.146	0.098	0.068
$\chi_p; \chi_e; \chi_s$	6.966e-4	0.008	0.096	0.441	0.777	522

**Table 3.** Comparisons of central kurtosis indices for IM broken rotor bar fault detection.

### 3.3.1. 35 Hz supply frequency

The proposed SS technique is first tested with stator current signals collected from an IM with the outer race defect, 35 Hz power supply frequency, and a light-load (20% of rated power). The settings for the proposed SS technique are selected as  $J = 20$ ,  $f_s = 65,500$  Hz,  $f_w = 10$  Hz, and  $f_v = 3.066 f_r$ . The high sampling frequency is used to accurately estimate the IM shaft speed. To obtain representative fault features, the frequency band [1000, 2000] Hz is selected for bearing fault detection.

To have a clear view of fault frequency components, the frequency band [1090, 1360] Hz from an IM with outer race bearing defect is shown in Figure 9 using PSD (Figure 9) and envelope analysis (Figure 9b). It is seen that the bearing fault frequency components are difficult to recognize due to the modulation of the signals with other IM frequency components.

The FIS, corresponding to a healthy IM and an IM with the outer race defect, are given in Figures 10(a) and 10(b), respectively. The values of indices corresponding to these three fault detection techniques are summarized in Table 4. It is seen from Figure 10 that the fault frequency component in Figure 10(b) protrudes more significantly than that in Figure 10(a). In Table 4, the fault index  $\chi_s$  of the IM with faulty bearing is greater than that of a healthy IM using the proposed SS technique, whereas the envelope analysis, associated with its index  $\chi_e$ , cannot recognize different IM health conditions. The PSD index  $\chi_p$  generates small values that cannot be relied on. Therefore, the SS technique can be used effectively for IM outer race bearing fault detection in this case, when compared to PSD and envelope analysis.

### 3.3.2. 50 Hz supply frequency

In this test, the IM supply frequency is set as 50 Hz. The other settings remain the same as in previous test. The frequency band [1000, 2000] Hz of an IM with an outer race bearing defect is used for testing. The band [1400, 1750] Hz is shown in Figure 11, using PSD (Figure 11a) and envelope analysis (Figure 11b), respectively. From Figure 11, the bearing fault frequency components in the spectrum are masked by higher amplitude frequency components unrelated to the bearings, which will degrade the fault detection reliability.

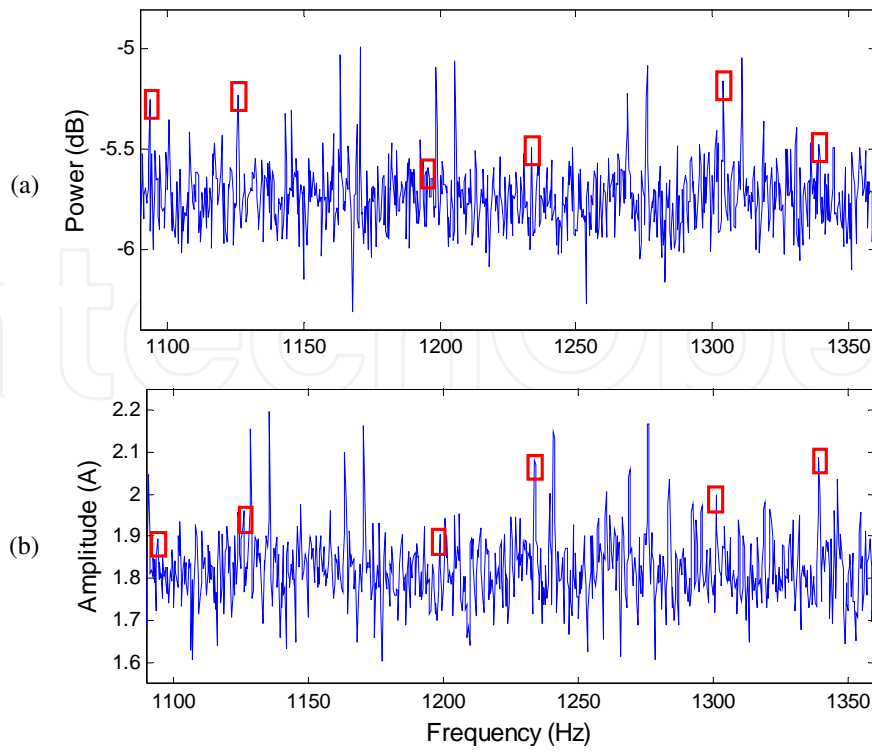


**Figure 9.** The spectrum average  $\Phi$  for an IM with outer race bearing defects, 35 Hz supply frequency, and light-load condition, using (a) PSD; and (b) envelope analysis. The rectangular boxes indicate bearing fault frequency components.

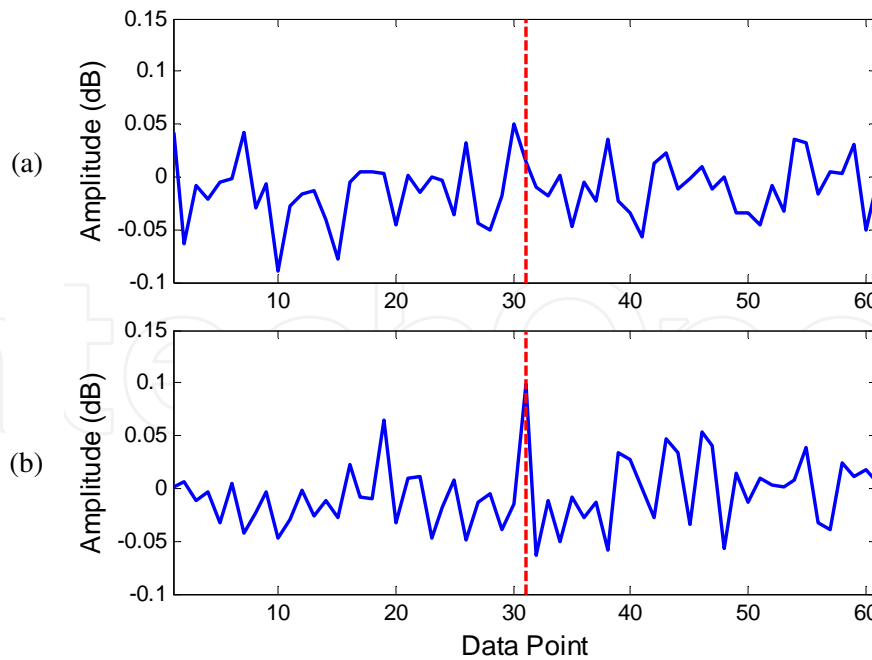


**Figure 10.** The FIS generated by the SS technique at 35 Hz supply frequency and with a light-load condition (a) from a healthy IM; (b) from an IM with outer race bearing defect.

Methods	PSD		Envelope analysis		SS	
Conditions	Healthy	Faulty	Healthy	Faulty	Healthy	Faulty
$f_r$	34.746	34.716	34.746	34.716	34.746	34.716
$v_p; v_e; v_s$	0	0.006	0	0	0.023	0.107
$\sigma_p; \sigma_e; \sigma_s$	0.203	0.161	0.102	0.081	0.029	0.029
$\chi_p; \chi_e; \chi_s$	0	1.929e-6	0	0	0.396	185

**Table 4.** Comparisons of central kurtosis indices for IM outer race bearing fault detection.

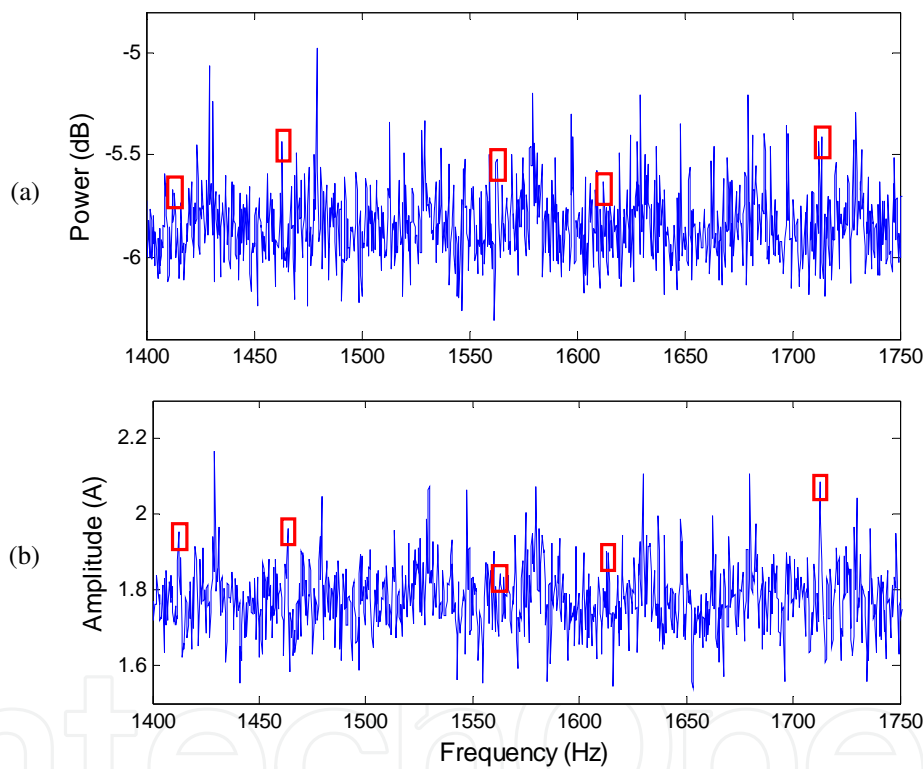


**Figure 11.** The spectrum average  $\Phi$  for an IM with outer race bearing defects, 50 Hz supply frequency, and light-load condition, using (a) PSD; and (b) envelope analysis.

The FIS of a healthy IM and an IM with outer race bearing defect are shown in Figure 12. The values of the shaft speed  $f_r$  and indices of the PSD, the envelope analysis and the proposed SS technique are listed in Table 5. It is seen that peaked center frequency component can be highlighted in Figure 12(b) than in Figure 12(a). From Table 5, it is seen that the values of  $\chi_s$  in the proposed SS technique are much greater than that from a healthy IM. Thus, the SS technique and its index  $\chi_s$  can be used for IM outer race bearing defect detection at different supply frequencies.

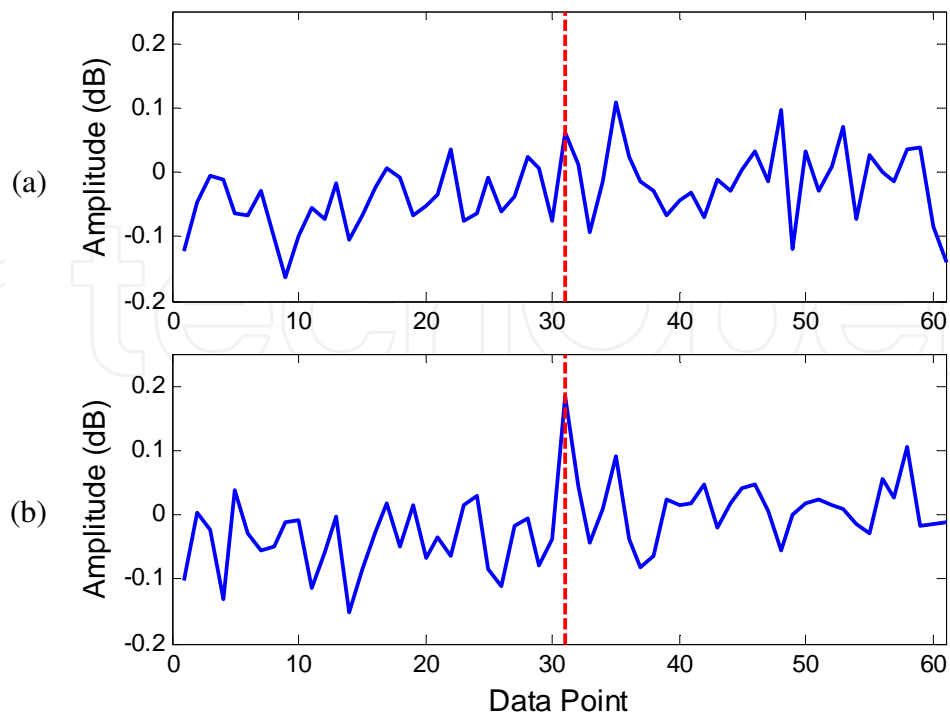


**Figure 12.** The FIS generated by the SS technique at 50 Hz supply frequency and light-load condition (a) from a healthy IM; (b) from an IM with an outer race bearing defect.

Methods	PSD		Envelope analysis		SS	
	Healthy	Faulty	Healthy	Faulty	Healthy	Faulty
$f_r$	49.757	49.705	49.757	49.705	49.757	49.705
$v_p; v_e; v_s$	0	0.041	0.005	0.007	0.090	0.196
$\sigma_p; \sigma_e; \sigma_s$	0.176	0.173	0.087	0.086	0.055	0.052
$\chi_p; \chi_e; \chi_s$	0	0.003	1.091e-5	4.389e-5	7.170	202

**Table 5.** Comparisons of central kurtosis indices for IM outer race bearing fault detection.

## 4. Conclusion

A spectrum synch, SS, technique has been proposed in this work for IM fault detection using electric current signals. This research focuses on broken rotor bar fault and outer race bearing fault detection. The local band synch technique is employed to synthesize bearing fault related features to form an FIS to enhance IM defect-related features. A central kurtosis analysis method is proposed to extract some features from the FIS, which are then used to formulate a

fault indicator. The effectiveness of the proposed IM fault detection technique is verified using IMs with the bearing defect and the broken rotor bar fault, under different operating conditions. Test results have shown that the proposed SS technique and the related central kurtosis indicator can capture IM defect features effectively and can provide more accurate IM health condition monitoring information. Further research is underway to improve its robustness of the SS technique and adopt it for fault detection in other IM components such as bearings with defects on inner races and rolling elements.

## Author details

Wilson Wang<sup>1\*</sup> and Derek Dezhi Li<sup>2</sup>

\*Address all correspondence to: [Wilson.Wang@Lakeheadu.ca](mailto:Wilson.Wang@Lakeheadu.ca)

1 Dept. of Mechanical Engineering, Lakehead University, Canada

2 Dept. of Mechanical and Mechatronics Engineering, University of Waterloo, Waterloo, Ontario, Canada

## References

- [1] Fei R., Fuchs E, Huang H: Comparison of two optimization techniques as applied to three-phase induction motor design. *IEEE Transaction on Energy Conversion*. 1989; 4:651-660.
- [2] Tavner P: Review of condition monitoring of rotating electrical machines. *IET Electrical Power Applications*. 2008; 2:215-247.
- [3] Okoro O: Steady and transient states thermal analysis of a 7.5-kW squirrel-cage induction machine at rated-load operation. *IEEE Transactions on Energy Conversion*. 2005; 20:730-736.
- [4] Widdle R, Krousgrill C, Sudhoff S: An induction motor model for high-frequency torsional vibration analysis. *Journal of Sound and Vibration*. 2006; 290:865-881.
- [5] Tandon N, Yadava G, Ramakrishna K: A comparison of some condition monitoring techniques for the detection of defect in induction motor ball bearings. *Mechanical Systems and Signal Processing*. 2007; 21:244-256.
- [6] Benbouzid M: A review of induction motors signature analysis as a medium for faults detection. *IEEE Transactions on Industrial Electronics*. 2000; 47:984-993.
- [7] Nandi S, Toliyat H, Li X: Condition monitoring and fault diagnosis of electrical motors – a review. *IEEE Transactions on Energy Conversion*. 2005; 20:719-729.

- [8] Thomson W, Fenger M: Current signature analysis to detect induction motor faults. *IEEE Industry Application Magazine*. 2001; 7:26-34.
- [9] Elkasabgy N, Eastham A, Dawson G: Detection of broken bars in the cage rotor on an induction machines. *IEEE Transactions on Industrial Applications*. 1992; 22:165-171.
- [10] Arabaci H, Bilgin O: The detection of rotor faults by using short time Fourier transform. *IEEE 15th Signal Processing and Communications Applications*. 2007; 1:1-4.
- [11] Ambardar A: *Analog and Digital Signal Processing*. Brooks/Cole Publishing Company; 1999.
- [12] Daviu J, Guasp M, Llinares J, Park J, Lee S, Yoo J, Kral C: Detection of broken outer-cage bars for double-Cage induction motors under the startup transient. *IEEE Transactions on Industry Applications*. 2012; 48:1539-1548.
- [13] Sadeghian A, Ye Z, Wu B: Online detection of broken rotor bars in induction motors by wavelet packet decomposition and artificial neural networks. *IEEE Transactions on Instrumentation and Measurement*. 2009; 8:2253-2263.
- [14] Pineda-Sanchez M, Riera-Guasp M, Roger-Folch J, Antonino-Daviu J, Perez-Cruz J, Puche-Panadero R: Diagnosis of induction motor faults in time-varying conditions using the polynomial-phase transform of the current. *IEEE Transactions on Industrial Electronics*. 2011; 58:1428-1439.
- [15] Riera-Guasp M, Pineda-Sanchez M, Perez-Cruz J, Puche-Panadero R, Roger-Folch J, Antonino-Daviu J: Diagnosis of induction motor faults via gabor analysis of the current in transient regime. *IEEE Transactions on Instrumentation and Measurement*. 2012; 61:1583-1596.
- [16] Akin A, Choi S, Orguner U, Toliyat H: A simple real-time fault signature monitoring tool for motor-drive-embedded fault diagnosis systems. *IEEE Transactions on Industrial Electronics*. 2011; 58:1990-2001.
- [17] Soualhi A, Clerc G, Razik H: Detection and diagnosis of faults in induction motor using an improved artificial ant clustering technique. *IEEE Transactions on Industrial Electronics*. 2013; 60:4053-4062.
- [18] Gunal S, Ece D, Gerek O: Induction machine condition monitoring using notch-filtered motor current. *Mechanical Systems and Signal Processing*. 2009; 23:2658-2670.
- [19] Blodt M, Granjon P, Raison B, Rostaing G: Models for bearing damage detection in induction motors using stator current monitoring. *IEEE Transactions on Industrial Electronics*. 2008; 55:1813-1822.
- [20] Tran V, Thobiani F, Ball A, Choi B: An application to transient current signal based induction motor fault diagnosis of Fourier-Bessel expansion and simplified fuzzy ARTMAP. *Expert Systems with Applications*. 2003; 4:5372-5384.

- [21] Devaney M, Eren L: Detecting motor bearing faults. *IEEE Instrumentation and Measurement Magazine*. 2004; 7:30-50.
- [22] Konar P, Vhattopadhyay P: Bearing fault detection of induction motor using wavelet and support vector machines. *Applied Soft Computing*. 2011; 11:4203-4211.
- [23] Lau E, Ngan H: Detection of motor bearing outer raceway defect by wavelet packet transformed motor current signature analysis. *IEEE Transactions on Instrumentation and Measurement*. 2010; 59:2683-2690.
- [24] Frosini L, Bassi E: Stator current and motor efficiency as indicators for different types of bearing faults in induction motors. *IEEE Transactions on Industrial Electronics*. 2010; 57:244-251.
- [25] Zhou W, Lu B, Habetler T, Harley R: Incipient bearing fault detection via motor stator current noise cancellation using Wiener filter. *IEEE Transactions on Industry Applications*. 2009; 45:1309-1317.
- [26] Romero-Troncoso R., et al.: FPGA-based online detection of multiple combined faults in induction motors through information entropy and fuzzy inference. *IEEE Transactions on Industrial Electronics*. 2011; 58:5263-5270.
- [27] Pineda-Sanchez M., et al.: Application of the Teager-Kaiser energy operator to the fault diagnosis of induction motors. *IEEE Transactions on Energy Conversion*. 2013; 28:1036-1044.
- [28] Press W, Teukolsky S, Vetterling W, Flannery B: *Numerical Recipes 3rd Edition: The Art of Scientific Computing*. Cambridge: Cambridge University Press; 2007.
- [29] Ilonen J, Kamarainen J, Lindh T, Ahola J, Kalviainen H, Partanen J: Diagnosis tool for motor condition monitoring. *IEEE Transactions on Industry Applications*. 2005; 41:963-971.

IntechOpen

